

Refractive index variance of cells and tissues measured by quantitative phase imaging

MINGGUANG SHAN,^{1,2} MIKHAIL E. KANDEL,¹ AND GABRIEL POPESCU^{1,*}

¹Quantitative Light Imaging Laboratory, Department of Electrical and Computer Engineering, Beckman Institute for Advanced Science and Technology, University of Illinois at Urbana-Champaign, Urbana, Illinois 61801, USA

²College of Information and Communication Engineering, Harbin Engineering University, Harbin, Heilongjiang 150001, China

*gpopescu@illinois.edu

Abstract: The refractive index distribution of cells and tissues governs their interaction with light and can report on morphological modifications associated with disease. Through intensity-based measurements, refractive index information can be extracted only via scattering models that approximate light propagation. As a result, current knowledge of refractive index distributions across various tissues and cell types remains limited. Here we use quantitative phase imaging and the statistical dispersion relation (SDR) to extract information about the refractive index variance in a variety of specimens. Due to the phase-resolved measurement in three-dimensions, our approach yields refractive index results without prior knowledge about the tissue thickness. With the recent progress in quantitative phase imaging systems, we anticipate that using SDR will become routine in assessing tissue optical properties.

© 2017 Optical Society of America

OCIS codes: (170.6935) Tissue characterization; (170.1530) Cell analysis; (180.3170) Interference microscopy; (290.5820) Scattering measurements; (050.1960) Diffraction theory.

References and links

1. V. V. Tuchin, *Tissue Optics: Light Scattering Methods and Instruments for Medical Diagnosis* (SPIE Press, 2007), Vol. 642.
2. A. Wax, C. Yang, M. G. Müller, R. Nines, C. W. Boone, V. E. Steele, G. D. Stoner, R. R. Dasari, and M. S. Feld, "In situ detection of neoplastic transformation and chemopreventive effects in rat esophagus epithelium using angle-resolved low-coherence interferometry," *Cancer Res.* **63**(13), 3556–3559 (2003).
3. A. Baumgartner, S. Dichtl, C. K. Hitzberger, H. Sattmann, B. Robl, A. Moritz, A. F. Fercher, and W. Sperr, "Polarization-sensitive optical coherence tomography of dental structures," *Caries Res.* **34**(1), 59–69 (1999).
4. M. E. Brezinski, G. J. Tearney, B. E. Bouma, J. A. Izatt, M. R. Hee, E. A. Swanson, J. F. Southern, and J. G. Fujimoto, "Optical coherence tomography for optical biopsy. Properties and demonstration of vascular pathology," *Circulation* **93**(6), 1206–1213 (1996).
5. K. Badizadegan, V. Backman, C. W. Boone, C. P. Crum, R. R. Dasari, I. Georgakoudi, K. Keefe, K. Munger, S. M. Shapshay, E. E. Sheetse, and M. S. Feld, "Spectroscopic diagnosis and imaging of invisible pre-cancer," *Faraday Discuss.* **126**, 265–311 (2004).
6. I. Georgakoudi, B. C. Jacobson, J. Van Dam, V. Backman, M. B. Wallace, M. G. Müller, Q. Zhang, K. Badizadegan, D. Sun, G. A. Thomas, L. T. Perelman, and M. S. Feld, "Fluorescence, reflectance, and light-scattering spectroscopy for evaluating dysplasia in patients with Barrett's esophagus," *Gastroenterology* **120**(7), 1620–1629 (2001).
7. A. Dhar, K. S. Johnson, M. R. Novelli, S. G. Bown, I. J. Bigio, L. B. Lovat, and S. L. Bloom, "Elastic scattering spectroscopy for the diagnosis of colonic lesions: initial results of a novel optical biopsy technique," *Gastrointest. Endosc.* **63**(2), 257–261 (2006).
8. V. Backman, R. Gurjar, K. Badizadegan, I. Itzkan, R. R. Dasari, L. T. Perelman, and M. S. Feld, "Polarized light scattering spectroscopy for quantitative measurement of epithelial cellular structures in situ," *IEEE J. Sel. Top. Quantum Electron.* **5**(4), 1019–1026 (1999).
9. K. Chen, L. T. Perelman, Q. Zhang, R. R. Dasari, and M. S. Feld, "Optical computed tomography in a turbid medium using early arriving photons," *J. Biomed. Opt.* **5**(2), 144–154 (2000).
10. A. Wax, C. Yang, V. Backman, M. Kalashnikov, R. R. Dasari, and M. S. Feld, "Determination of particle size by using the angular distribution of backscattered light as measured with low-coherence interferometry," *J. Opt. Soc. Am. A* **19**(4), 737–744 (2002).

11. I. J. Bigio, S. G. Bown, G. Briggs, C. Kelley, S. Lakhani, D. Pickard, P. M. Ripley, I. G. Rose, and C. Saunders, "Diagnosis of breast cancer using elastic-scattering spectroscopy: preliminary clinical results," *J. Biomed. Opt.* **5**(2), 221–228 (2000).
12. R. Drezek, M. Guillaud, T. Collier, I. Boiko, A. Malpica, C. Macaulay, M. Follen, and R. Richards-Kortum, "Light scattering from cervical cells throughout neoplastic progression: influence of nuclear morphology, DNA content, and chromatin texture," *J. Biomed. Opt.* **8**(1), 7–16 (2003).
13. J. R. Mourant, T. M. Johnson, S. Carpenter, A. Guerra, T. Aida, and J. P. Freyer, "Polarized angular dependent spectroscopy of epithelial cells and epithelial cell nuclei to determine the size scale of scattering structures," *J. Biomed. Opt.* **7**(3), 378–387 (2002).
14. A. Pifferi, J. Swartling, E. Chikoidze, A. Torricelli, P. Taroni, A. Bassi, S. Andersson-Engels, and R. Cubeddu, "Spectroscopic time-resolved diffuse reflectance and transmittance measurements of the female breast at different interfiber distances," *J. Biomed. Opt.* **9**(6), 1143–1151 (2004).
15. B. W. Pogue, S. Jiang, H. Dehghani, C. Kogel, S. Soho, S. Srinivasan, X. Song, T. D. Tosteson, S. P. Poplack, and K. D. Paulsen, "Characterization of hemoglobin, water, and NIR scattering in breast tissue: analysis of intersubject variability and menstrual cycle changes," *J. Biomed. Opt.* **9**(3), 541–552 (2004).
16. H. W. Wang, T. C. Zhu, M. E. Putt, M. Solonenko, J. Metz, A. Dimofte, J. Miles, D. L. Fraker, E. Glatstein, S. M. Hahn, and A. G. Yodh, "Broadband reflectance measurements of light penetration, blood oxygenation, hemoglobin concentration, and drug concentration in human intraperitoneal tissues before and after photodynamic therapy," *J. Biomed. Opt.* **10**(1), 014004 (2005).
17. A. Wax, J. W. Pyhtila, R. N. Graf, R. Nines, C. W. Boone, R. R. Dasari, M. S. Feld, V. E. Steele, and G. D. Stoner, "Prospective grading of neoplastic change in rat esophagus epithelium using angle-resolved low-coherence interferometry," *J. Biomed. Opt.* **10**(5), 051604 (2005).
18. A. Amelink, D. J. Robinson, and H. J. Sterenborg, "Confidence intervals on fit parameters derived from optical reflectance spectroscopy measurements," *J. Biomed. Opt.* **13**(5), 054044 (2008).
19. K. Bizheva, A. Unterhuber, B. Hermann, B. Povazay, H. Sattmann, A. F. Fercher, W. Drexler, M. Preusser, H. Budka, A. Stingl, and T. Le, "Imaging ex vivo healthy and pathological human brain tissue with ultra-high-resolution optical coherence tomography," *J. Biomed. Opt.* **10**(1), 011006 (2005).
20. R. Choe, S. D. Konecky, A. Corlu, K. Lee, T. Durduran, D. R. Busch, S. Pathak, B. J. Czerniecki, J. Tchou, D. L. Fraker, A. Demichele, B. Chance, S. R. Arridge, M. Schweiger, J. P. Culver, M. D. Schnall, M. E. Putt, M. A. Rosen, and A. G. Yodh, "Differentiation of benign and malignant breast tumors by in-vivo three-dimensional parallel-plate diffuse optical tomography," *J. Biomed. Opt.* **14**(2), 024020 (2009).
21. D. J. Cuccia, F. Bevilacqua, A. J. Durkin, F. R. Ayers, and B. J. Tromberg, "Quantitation and mapping of tissue optical properties using modulated imaging," *J. Biomed. Opt.* **14**(2), 024012 (2009).
22. S. L. Jacques and B. W. Pogue, "Tutorial on diffuse light transport," *J. Biomed. Opt.* **13**(4), 041302 (2008).
23. A. Roggan, M. Friebel, K. Do Rschel, A. Hahn, and G. Mu Ller, "Optical Properties of Circulating Human Blood in the Wavelength Range 400-2500 nm," *J. Biomed. Opt.* **4**(1), 36–46 (1999).
24. B. J. Tromberg, N. Shah, R. Lanning, A. Cerussi, J. Espinoza, T. Pham, L. Svaasand, and J. Butler, "Non-invasive in vivo characterization of breast tumors using photon migration spectroscopy," *Neoplasia* **2**(1-2), 26–40 (2000).
25. V. Ntziachristos, X. H. Ma, A. G. Yodh, and B. Chance, "Multichannel photon counting instrument for spatially resolved near infrared spectroscopy," *Rev. Sci. Instrum.* **70**(1), 193–201 (1999).
26. R. S. Gurjar, V. Backman, L. T. Perelman, I. Georgakoudi, K. Badizadegan, I. Itzkan, R. R. Dasari, and M. S. Feld, "Imaging human epithelial properties with polarized light-scattering spectroscopy," *Nat. Med.* **7**(11), 1245–1248 (2001).
27. S. L. Jacques, "Optical properties of biological tissues: a review," *Phys. Med. Biol.* **58**(11), R37–R61 (2013).
28. G. Popescu, *Quantitative Phase Imaging of Cells and Tissues* (McGraw-HillNew York, 2011).
29. S. Uttam, H. V. Pham, J. LaFace, B. Leibowitz, J. Yu, R. E. Brand, D. J. Hartman, and Y. Liu, "Early prediction of cancer progression by depth-resolved nanoscale maps of nuclear architecture from unstained tissue specimens," *Cancer Res.* **75**(22), 4718–4727 (2015).
30. S. Sridharan, V. Macias, K. Tangella, A. Kajdacsy-Balla, and G. Popescu, "Prediction of prostate cancer recurrence using quantitative phase imaging," *Sci. Rep.* **5**, 9976 (2015).
31. H. Majeed, M. E. Kandel, K. Han, Z. Luo, V. Macias, K. Tangella, A. Balla, and G. Popescu, "Breast cancer diagnosis using spatial light interference microscopy," *J. Biomed. Opt.* **20**(11), 111210 (2015).
32. Z. Wang, K. Tangella, A. Balla, and G. Popescu, "Tissue refractive index as marker of disease," *J. Biomed. Opt.* **16**(11), 116017 (2011).
33. H. Ding, Z. Wang, X. Liang, S. A. Boppart, K. Tangella, and G. Popescu, "Measuring the scattering parameters of tissues from quantitative phase imaging of thin slices," *Opt. Lett.* **36**(12), 2281–2283 (2011).
34. Z. Wang, H. Ding, and G. Popescu, "Scattering-phase theorem," *Opt. Lett.* **36**(7), 1215–1217 (2011).
35. Z. Wang, D. L. Marks, P. S. Carney, L. J. Millet, M. U. Gillette, A. Mihi, P. V. Braun, Z. Shen, S. G. Prasanth, and G. Popescu, "Spatial light interference tomography (SLIT)," *Opt. Express* **19**(21), 19907–19918 (2011).
36. Z. Wang, L. Millet, M. Mir, H. Ding, S. Unarunotai, J. Rogers, M. U. Gillette, and G. Popescu, "Spatial light interference microscopy (SLIM)," *Opt. Express* **19**(2), 1016–1026 (2011).
37. M. Shan, V. Nastasa, and G. Popescu, "Statistical dispersion relation for spatially broadband fields," *Opt. Lett.* **41**(11), 2490–2492 (2016).

38. T. Kim, R. Zhou, M. Mir, S. D. Babacan, P. S. Carney, L. L. Goddard, and G. Popescu, "White-light diffraction tomography of unlabeled live cells," *Nat. Photonics* **8**(3), 256–263 (2014).
39. E. Cuche, F. Bevilacqua, and C. Depeursinge, "Digital holography for quantitative phase-contrast imaging," *Opt. Lett.* **24**(5), 291–293 (1999).
40. Y. Sung, W. Choi, C. Fang-Yen, K. Badizadegan, R. R. Dasari, and M. S. Feld, "Optical diffraction tomography for high resolution live cell imaging," *Opt. Express* **17**(1), 266–277 (2009).
41. M. Lee, E. Lee, J. Jung, H. Yu, K. Kim, J. Yoon, S. Lee, Y. Jeong, and Y. Park, "Label-free optical quantification of structural alterations in Alzheimer's disease," *Sci. Rep.* **6**, 31034 (2016).

1. Introduction

Refractive index distribution is an intrinsic property of tissues, which governs light matter interaction and has shown potential for label-free diagnosis [1]. As a result, light scattering techniques for tissue diagnosis have long been used in various configurations (see, e.g., Refs [2–26]). The measurable quantity is typically the irradiance as a function of the momentum transfer, $q = 2\pi\sin(\theta/2)\lambda$, where λ is the wavelength of the light in the tissue and θ is the scattering angle, Fig. 1. Thus, two classes of scattering measurements have emerged: spectroscopic, and angular, depending on whether, respectively, the λ -dependence or θ -dependence is retrieved experimentally. The experimental curves are fitted with a physical model that contains particular assumptions about the light-tissue integration, e.g., the first-order Born approximation, for weakly scattering regime, and the diffusion approximation for strong multiple scattering. Often, the tissue is approximated by a distribution of spheres, for which Mie theory results can be computed easily [27].

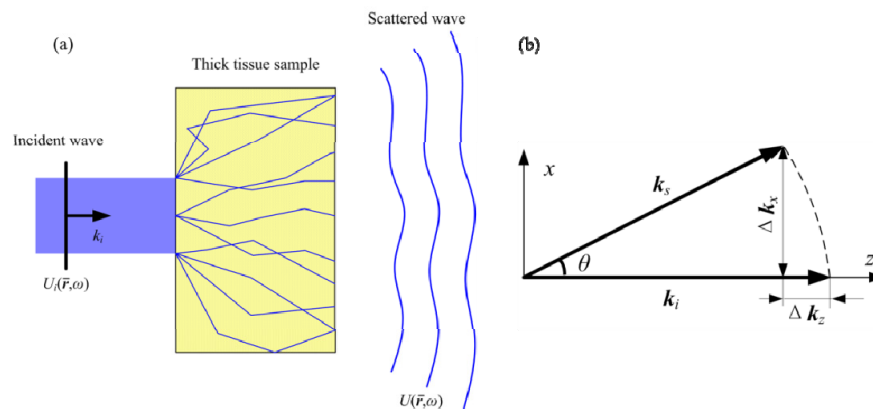


Fig. 1. (a) Scattering geometry, U_i , k_i are the incident field and wavevector. (b) Momentum conservation: k_i and k_s are the incident and scattered wave vector, Δk_x and Δk_z are the variance of the components of the transverse wave vector, θ is the scattering angle.

Quantitative phase imaging (QPI) [28] has been applied recently to imaging tissue slices, including unlabeled biopsies [29–32]. The phase maps obtained made it evident that, at least in the visible domain, tissue structure is better described by a continuous distribution of refractive index rather than a discrete ensemble of particles. These findings led to the development of light tissue scattering models based on the first-order Born approximation [33, 34]. It has been demonstrated that QPI based on spatial light interference microscopy (SLIM) [35, 36] can be used for diagnosis and prognosis in unlabeled cancer biopsies [30, 32]. Still, measuring the refractive index from a QPI image requires knowledge of the tissue thickness. Thus, despite significant progress, measuring information about the tissue refractive index distribution remains a grand challenge.

Here we present a new approach for extracting cell and tissue refractive index information from QPI data.

2. Theory

We use the statistical dispersion relation (SDR) [37] and experimental results from QPI to extract information about the refractive index distribution of cells and tissues. The dispersion relation associated with a field in weakly scattering medium, has the form (see Ref [37]. for the proof)

$$\langle k^2 \rangle = n_0^2 \beta_0^2 \left(1 + \frac{\sigma_n^2}{n_0^2} \right) \quad (1)$$

In Eq. (1), $\langle k^2 \rangle$ is the second order moment of the wavevector, $\langle k^2 \rangle = \langle k_x^2 \rangle + \langle k_y^2 \rangle + \langle k_z^2 \rangle$, angular brackets denote ensemble averaging, n_0 is average refractive index, β_0 is the wavenumber in vacuum, $\beta_0 = \omega/c$, and σ_n^2 is the variance of the refractive index in the 3D volume. Our goal is to use QPI data, from which to obtain $\langle k^2 \rangle$, and use Eq. (1) to extract σ_n^2 .

In order to measure optical path length maps associated with thin biological specimens, we exploited SLIM [35, 36], which provides phase information with high sensitivity. The SLIM system (Cell Vista SLIM Pro, Phi Optics, Inc.) benefits from a common path interferometric geometry and white light illumination, which grant excellent temporal and spatial sensitivity [36]. The measureable quantity is the phase of the temporal cross-correlation function, evaluated at the origin [38], namely

$$\begin{aligned} \Gamma_{01}(\mathbf{r}) &= \langle U_0^*(\mathbf{r}, t) U_1(\mathbf{r}, t + \tau) \rangle \Big|_{\tau=0} \\ &= |\Gamma_{01}(\mathbf{r})| e^{i\phi(\mathbf{r})} \end{aligned} \quad (2)$$

In Eq. (2), U_0 is the reference field, $U_0 = A_0 e^{in_0 \beta_0 z}$, U_1 is the image field, and ϕ represents the measureable phase shift.

In order to compute the second order moment of the wavevector from the measured ϕ , we start with the definition of $\langle k^2 \rangle$, which reads

$$\begin{aligned} \langle k^2 \rangle &= \frac{\int k^2 |U(\mathbf{k})|^2 d^3 \mathbf{k}}{\int |U(\mathbf{k})|^2 d^3 \mathbf{k}} \\ &= \frac{\int (k_x^2 + k_y^2 + k_z^2) |U(\mathbf{k})|^2 d^3 \mathbf{k}}{\int |U(\mathbf{k})|^2 d^3 \mathbf{k}}. \end{aligned} \quad (3)$$

From Parseval's theorem we have the following identity

$$\int |U(\mathbf{k}, \omega)|^2 d^3 \mathbf{k} = 8\pi^3 \int |U(\mathbf{r}, \omega)|^2 d^3 \mathbf{r}. \quad (4)$$

Furthermore, we use the differentiation property of the Fourier transform,

$$k_x U(\mathbf{k}, \omega) \leftrightarrow \frac{1}{i} \frac{\partial U(\mathbf{r}, \omega)}{\partial x} \quad (5)$$

where \leftrightarrow indicates the Fourier transformation. Equation (5) allows us to express k_x^2 in terms of the derivative along x , while Eq. (4) can be used to replace the integrals over \mathbf{k} with ones over \mathbf{r} . Thus, Eq. (3) can be re-written as

$$\langle k_x^2 \rangle = \frac{\int \left| \frac{\partial U(\mathbf{r}, \omega)}{\partial x} \right|^2 d^3 \mathbf{r}}{\int |U(\mathbf{r}, \omega)|^2 d^3 \mathbf{r}}. \quad (6)$$

For phase objects, the measured field from the specimen can be expressed as

$$U(\mathbf{r}, \omega) = A(\omega) \exp[i\phi(\mathbf{r})], \quad (7)$$

where A is the amplitude of the field. As a result, Eq. (6) takes a simple form,

$$\langle k_x^2 \rangle = \int \left| \frac{\partial \phi(\mathbf{r}, \omega)}{\partial x} \right|^2 d^3 \mathbf{r}. \quad (8)$$

The same process applies to the y and z dimensions, such that, finally, the variance of the refractive index associated with a transparent specimen, can be retrieved from the measured phase image as

$$\sigma_n^2 = \frac{1}{\beta_0^2} \langle |\nabla \phi|^2 \rangle \quad (9)$$

In essence, Eq. (9) shows that we can extract the refractive index variance from the mean gradient intensity of the measured phase images.

3. Results

In order to illustrate this approach, we present experimental results on live neurons and a number of tissue biopsies. We used white light from a halogen lamp, with central wavelength of 574nm and full-width half maximum of 150nm, and a 40X /0.75 NA objective. Figure 2 shows results obtained on live neurons in culture. We measured a z -stack including 129 slices with a step of 9.0 slices/ μm , which matches our x - y sampling. Figure 2(a) shows a middle frame (1776 pixels \times 1760 pixels) of the z -stack reconstructed phase maps, while Figs. 2(b) and 2(c) show the first order derivative along x , $\partial\phi(\mathbf{r}, \omega)/\partial x$, and the gradient intensity along x , i.e., $|\partial\phi(\mathbf{r}, \omega)/\partial x|^2$, respectively. Figure 2(d) shows the histogram of the gradient intensity with respect to x . Following Eq. (9), we can calculate the second order moment of the \mathbf{k} -vector of $\langle k_x^2 \rangle$, $\langle k_y^2 \rangle$ and $\langle k_z^2 \rangle$ in the whole field of view and then calculate the spatial variance of refractive index, σ_n . We can apply the same approach to regions of interest of arbitrary size in the field of view.

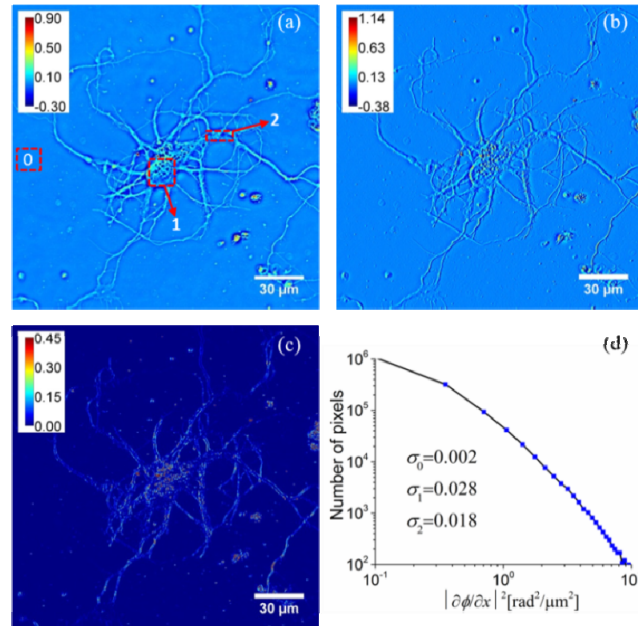


Fig. 2. (a) SLIM image of a neuron, with the color bar indicates phase in radians (Visualization 1). (b) Map of $\frac{\partial\phi}{\partial x}$, with the color bar indicates phase in units of $\text{rad}/\mu\text{m}$. (c) Map of $\left|\frac{\partial\phi}{\partial x}\right|^2$, with the color bar indicates phase in units of $(\text{rad}/\mu\text{m})^2$ (Visualization 2). (d) Histogram of the values in (c).

In Fig. 2, we show the σ_n results for a region on the neuron cell body vs. its neurites. The results indicate that the soma is characterized by a higher variance, $\sigma_1 = 0.028$ vs. $\sigma_2 = 0.018$. This difference can be attributed to the fact that neurites are essentially 1D structures, while the cell bodies are 2D. Note that the background generates an order of magnitude lower value for a comparable region, $\sigma_0 = 0.002$. This σ_0 value ideally would approach zero for a noise free measurement. However, spatial phase noise due to the optics and impurities in the cell culture contribute to a non-zero background level, which represents the ultimate sensitivity of our measurement.

We further applied our approach to measure colon biopsies, of $6 \mu\text{m}$ thickness. The z-stack consisting of 300 slices was recorded using the SLIM instrument, at the same axial sampling as before. Following the same procedure, we obtained the refractive index variance over the whole field of view of $\sigma_n = 0.026$, as shown in Fig. 3. Again, choosing different regions of interests yields different values of the variance, which indicates the strong refractive index inhomogeneity associated with the tissue.

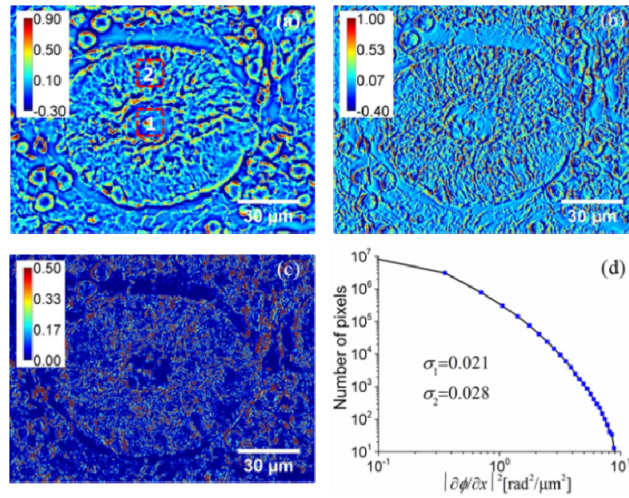


Fig. 3. (a) SLIM image of a colon biopsy, with the color bar indicating phase in radians (Visualization 3). (b) Map of $\frac{\partial\phi}{\partial x}$, with the color bar indicating phase in units of $\text{rad}/\mu\text{m}$. (c) Map of $\left|\frac{\partial\phi}{\partial x}\right|^2$, with the color bar indicates phase in units of $(\text{rad}/\mu\text{m})^2$ (Visualization 4). (d) Histogram of the values in (c).

We performed the same analysis on 8 distinct regions of colon tissue slice and summarized their results in Fig. 4. The refractive index variance, averaged over the 8 measurements, is $\sigma_n = 0.023 \pm 0.006$.

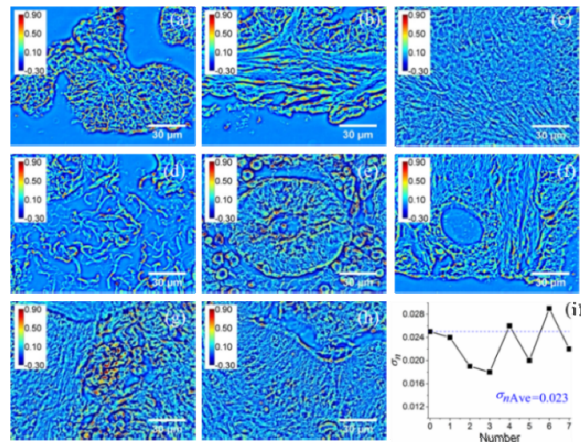


Fig. 4. (a)-(h) SLIM images of different colon biopsies, with the color bar indicating phase in radians. (i) the refractive index variance σ_n for (a)-(h).

We also acquired z-stacks of papillary thyroid cancer biopsies. The z-stack consisted of 300 frames and one of the retrieved phase maps ($2064 \text{ pixels} \times 2048 \text{ pixels}$) is shown in Fig. 5(a). The results obtained for the first-order derivative and its magnitude squared with respect to x are shown in Fig. 5(b) and 5(c). The histogram of the gradient intensity is shown in Fig. 5(d). The refractive index variance in the whole field is $\sigma_n = 0.029$, and the selected areas show slight variations around this value.

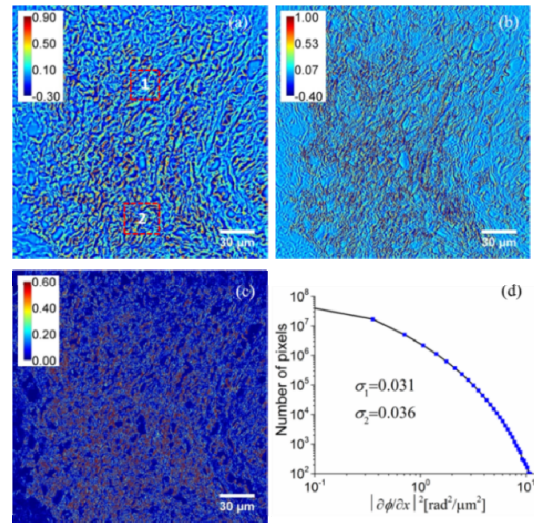


Fig. 5. (a) SLIM image of a papillary thyroid cancer biopsy, with the color bar indicating phase in radians (Visualization 5). (b) Map of $\frac{\partial\phi}{\partial x}$, with the color bar indicating phase in units of rad/ μm . (c) Map of $\left|\frac{\partial\phi}{\partial x}\right|^2$, with the color bar indicates phase in units of $(\text{rad}/\mu\text{m})^2$ (Visualization 6). (d) Histogram of the values in (c).

Different papillary thyroid cancer biopsies are shown in Figs. 6(a)-6(h), and their relevant refractive index variances are presented in Fig. 6(i). The refractive index variance averaged over all the measurements is $\sigma_n = 0.021 \pm 0.008$.

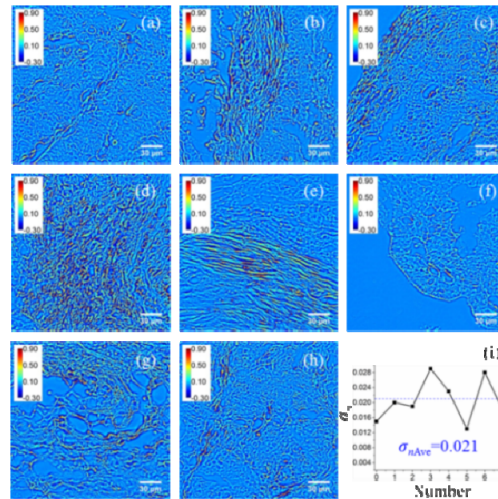


Fig. 6. (a)-(h) SLIM images of different papillary thyroid cancer biopsies, with the color bar indicates phase in radians. (i) the refractive index variance σ_n for (a)-(h)

4. Summary and discussion

In summary, three-dimensional QPI data can be used to extract the variance of the refractive index in cells and tissues. The key feature of this approach is that the thickness of the specimen is not required a priori. This is due to the use of the SDR, which only requires that the sample of interest is sampled in its entirety and the results averaged properly. One

important difference with respect to the tomographic approaches [38–40] is that SDR does not require solving the scattering inverse problem, i.e., we retrieve the variance of the refractive index, not its 3D distribution. As a result, this method is very fast and practical. For weakly scattering objects, such as cells and thin slices of tissue, the refractive index variance can be simply obtained from the gradient of the phase data. The amplitude modulation is likely to make a difference in brain slices, as reported in Ref. 41. However, in all our live cell and unstained biopsy imaging, amplitude modulation is negligible, which justifies our approximation of phase objects. Although a measure of the refractive distribution spread and not of the absolute values of refractive index, the variance has been shown to be crucial when diagnosing diseases such as cancer [31]. It is possible that during cancer progression the average value of the tissue refractive index may not change, but its spatial distribution undergoes modification [31]. Because of the tremendous progress in QPI instrumentation, we hope that the approach presented here will be readily adopted to extract information about optical properties of biomedical specimens.

Funding

National Science Foundation (CBET-0939511 STC, DBI 14-50962 EAGER, IIP-1353368) (for more information, visit <http://light.ece.illinois.edu/>); National Natural Science Foundation of China (NSFC) (61377009); Major National Scientific Instrument and Equipment Development Project of China (2013YQ290489); China Scholarship Council (201506685053); Heilongjiang Science Foundation of China (F201411); and Fundamental Research Funds for the Central Universities of China.

Acknowledgments

Neurons were prepared by Dr. Catherine Best at University of Illinois at Urbana-Champaign. The biopsy samples were prepared at the University of Illinois at Chicago under the supervision of Dr. Andre A. Kajdacsy-Balla.